On the Feasibility of Nanocrystal Imaging Using Intense and Ultrashort X-ray Pulses

Carl Caleman,[†,‡] Gösta Huldt,[§] Filipe R. N. C. Maia,[§] Carlos Ortiz,[⊥] Fritz G. Parak,[†] Janos Hajdu,[§] David van der Spoel,[§] Henry N. Chapman,[‡,¶] and Nicuşor Timneanu[§,*]

[†]Physik Department E17, Technische Universität München, James-Franck-Strasse, DE-85748 Garching, Germany, [‡]Center for Free-Electron Laser Science, DESY, Notkestrasse 85, DE-22607 Hamburg, Germany, [§]Department of Cell and Molecular Biology, Biomedical Centre, Box 596, Uppsala University, SE-75 124 Uppsala, Sweden, [⊥]Institut für Theoretische Physik, Goethe-Universität Frankfurt, Max-von-Laue-Strasse 1, DE-60438 Frankfurt am Main, Germany, and [¶]University of Hamburg, Luruper Chaussee 149, DE-22761 Hamburg, Germany

ABSTRACT Structural studies of biological macromolecules are severely limited by radiation damage. Traditional crystallography curbs the effects of damage by spreading damage over many copies of the molecule of interest in the crystal. X-ray lasers offer an additional opportunity for limiting damage by out-running damage processes with ultrashort and very intense X-ray pulses. Such pulses may allow the imaging of single molecules, clusters, or nanoparticles. Coherent flash imaging will also open up new avenues for structural studies on nano- and microcrystalline substances. This paper addresses the theoretical potentials and limitations of nanocrystallography with extremely intense coherent X-ray pulses. We use urea nanocrystals as a model for generic biological substances and simulate the primary and secondary ionization dynamics in the crystalline sample. The results establish conditions for ultrafast single-shot nanocrystallography diffraction experiments as a function of X-ray fluence, pulse duration, and the size of nanocrystals. Nanocrystallography using ultrafast X-ray pulses has the potential to open up a new route in protein crystallography to solve atomic structures of many systems that remain inaccessible using conventional X-ray sources.

KEYWORDS: X-ray free electron laser · nanocrystallography · radiation damage · molecular dynamics · coherent diffraction imaging

New light sources have had a significant influence on natural sciences. Radio transmitters, X-ray sources, and optical lasers triggered fundamental transformations both in science and society. As a consequence, expectations are high regarding the impact of the long-awaited first hard X-ray lasers. These lasers produce ultrashort and extremely intense coherent X-ray pulses with a peak brilliance exceeding that of conventional synchrotron sources by more than a billion. The FLASH soft X-ray free-electron laser in Germany[1] was the first instrument to reach into X-ray frequencies, and it is a fully operational user facility today. The LINAC Coherent Light Source (LCLS)[2] in the USA is a hard X-ray laser that has now produced first light and is lasing at 1.5 Å. Similar projects are under way in Japan[3] and in Europe.[4] In addition to these linear accelerator-based machines, table-top X-ray lasers, driven by optical lasers, have started making their mark.[5−7] Short, intense, coherent, hard X-ray pulses can be exploited for new experiments in disciplines ranging from experimental astrophysics to structural biology. Such X-ray pulses could open the door to single molecule imaging, that is, retrieving atomic structures from large biomolecules without the need of a crystalline sample.[8]

Three dimensional structures could also be determined from nanocrystalline materials. In the process of crystallization, many macromolecules fail to form large crystals (*e.g.*, membrane proteins). However, they often form submicrometer crystals, but these are usually too small to generate useful diffraction data at a conventional synchrotron source. It has been suggested[9−11] that such nanocrystals could be used for structural studies with X-ray lasers.

Any sample exposed to an intense X-ray pulse will be ionized, and extensive ionization destroys the sample. The time scale on which this process occurs is critical for obtaining an interpretable diffraction pattern to yield an atomic structure of the sample. In principle, the X-ray pulse must be short enough such that the entire pulse passes through the sample before a major disarrangement of the atomic and electronic configurations takes place. The ionizations due to direct photoabsorption and subsequent secondary processes affect the ability to get useful structural information from the diffraction pattern in three ways: (i) Ionization decreases the elastic X-ray scattering power of atoms. (ii) Removal of electrons from atoms leaves behind positively

*Address correspondence to nicusor@xray.bmc.uu.se.

Received for review August 4, 2010 and accepted November 27, 2010.

Published online December 7, 2010. 10.1021/nn1020693

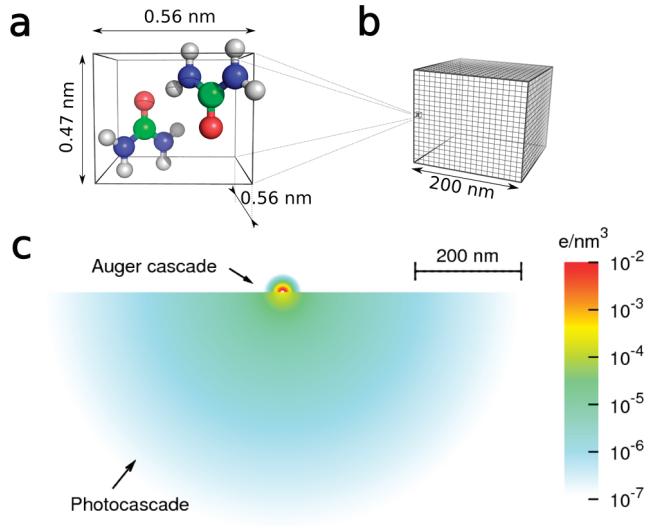

Figure 1. Comparison of crystal size and the modeled size of secondary electron cascades. (a) The unit cell of a urea crystal contains light elements abundant in proteins: carbon (depicted as green), nitrogen (blue), oxygen (red), and hydrogen (white). (b) A urea nanocrystal of 200 nm would contain about 50 million unit cells. A protein nanocrystal of similar size would contain about 20000 unit cells (using lysozyme as an example). (c) The overall dimensions of simulated electron clouds produced during the thermalization of a single 0.4 keV Auger electron ejected from a nitrogen atom (top) and a single 8 keV photoelectron (bottom) inside a large urea crystal after 50 fs. Similar cascade sizes are produced in protein crystals, during an X-ray diffraction experiment.

charged ions that repel each other due to Coulomb forces, leading to the destruction of the structure. (iii) Free electrons either leave the sample, if their energy is high enough, or remain in the sample as a background electron gas, in which case they will contribute to noise in the diffraction pattern.

There are currently no experiments on the dynamics of radiation damage from X-ray free-electron lasers (XFEL) at Ångström wavelengths. Experimental data published so far reach into the soft X-ray regime (to 13.5 nm wavelength).[12−14] Theoretical models extend the picture into the unexplored hard X-ray regime.[8,15−17]

The explosion mechanism strongly depends on sample size. Electrons ejected from atoms during exposure propagate through the sample and cause further ionization by eliciting secondary electron clouds. The extent of ionization through this mechanism is size dependent. Photoelectrons released by X-rays of 1.5 Å wavelength are fast (53 nm/fs), and they can escape from small samples such as "nanosized" crystals[18,19] or single protein molecules, early in an exposure. In contrast, Auger electrons are slow (9.5 nm/fs for carbon[20]) and calculations show that they will cause secondary ionization even in a single protein molecule.[15,21] Figure 1 illustrates the relevant size domain for the secondary electron cloud generated by a photoelectron and the respective cloud originating from the Auger electron in comparison with the size of a nanocrystal. In the late phase of an exposure, a significant fraction of the emitted electrons will not be able to escape the increased positive potential of the sample. It has been theoretically shown that for small samples (diameter < 10 nm), the explosion is dominated by Coulomb processes.[15] This is driven by the repulsion of the positive ions left behind by electrons leaving the sample. In big samples (diameter > 500 nm), most electrons will be trapped simply because they lose energy before reaching the surface. Trapped electrons increase the temperature of the sample through collisional processes, while slowing the Coulomb explosion by partially screening the positive charges and creating a net neutral core. Predictions point to a transition from Coulomb explosion to a hydrodynamic explosion with increasing sample size. A positively charged surface layer is formed and peels off, destroying the sample from outside toward the center. The expansion of the core is driven by thermal processes as the electron pressure grows.[16]

The aim of this theoretical work is to predict the damage caused by ionization in nanocrystals of biological material, with sizes up to one micrometer. Crystals larger than one micrometer are normally considered viable and diffract well enough at conventional synchrotron sources. We provide a theoretical screening tool for nanocrystallography experiments with regard to feasible sample sizes and X-ray laser pulse parameters. Serial crystallography experiments with submicrometer protein crystals have recently been performed at a synchrotron[22] and showed that powder diffraction data can be obtained using a continuous microjet of nanocrystals. It has also been theorized that longitudinal coherence properties of the X-ray lasers limit the resolution of single-particle diffraction imaging,[23] and it has been suggested that submicrometer samples are required to achieve atomic resolution at LCLS.

Descriptions of electron impact ionization and secondary ionization cascades exist for different materials.[21,24,25] Dynamics of photoelectrons in protein crystals have been investigated earlier,[18,19] without consideration to Auger emission or secondary ionization cascades. These predictions suggest that radiation damage can be limited by reducing the crystal size. The present work steps beyond these studies and gives an integrated description of photoemission, Auger emission, and cascade processes during exposure of a biological nanocrystal to an ultrashort and intense X-ray pulse, to determine the feasibility of nanocrystal imaging and improvement in resolution achievable with shorter pulses. Our findings are summarized in Figures 1−6, and the methodology is described in Methods section and in the Supporting Information.

RESULTS AND DISCUSSION

Figure 1 shows the simulated free electron distributions due to a single photoionization in an infinitely large urea crystal caused by a 1.5 Å photon. If a nanocrystal is smaller than the ionization cascades, most photoelectrons will leave the sample before thermaliza-

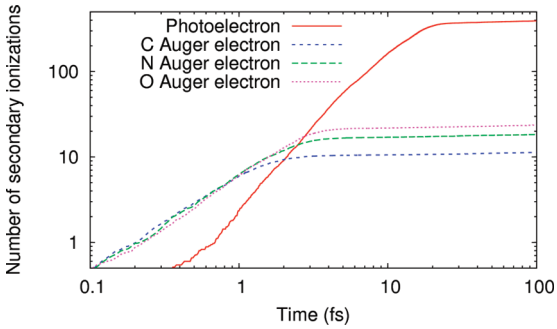

Figure 2. Evolution of secondary ionization cascades in a urea crystal. Number of secondary ionizations produced by a photoelectron of 8 keV and by Auger electrons (impact energies: 250 eV for carbon, 400 eV for nitrogen, 500 eV for oxygen) is shown as a function of time. Figure shows averaging over 1000 simulations on an infinitely large urea crystal.

tion. In a stepwise approach, we first treat the thermalization of electrons with various energies, corresponding to photoelectrons or different Auger electrons in urea. In the next step, we combine the primary and secondary ionization effects to describe the entire dynamics of the system during and after the X-ray pulse (Methods, eq 2). A detailed description of the model, electron scattering on atoms, treatment of electron−hole recombinations and electron−phonon interactions is presented in ref 21 and in the Supporting Information.

For light elements, a single photoionization releases electrons at two distinctly different energies (Figure 1). The photoelectron energy corresponds to the difference between the photon energy (8.3 keV corresponding to 1.5 Å wavelength) and the K-shell binding energy, while Auger electrons carry kinetic energy dependent on atom type. Auger energies for carbon, nitrogen, and oxygen in the urea target are approximately 250, 400, and 500 eV, respectively, which is more than an order of magnitude lower than the energy of the photoelectron. In the energy range considered here, the number of secondary ionizations produced by the inelastic scattering of a single electron scales linearly with the energy of the initial electron.[21,24] In Figure 1 the total number of ionizations was 18 in the complete Auger cascade, and 390 in the photoelectron cascade at 50 fs after the emission of primary electrons. At this point, the radius of gyration of the photoelectron cloud reached 300 nm, and that of the Auger electron cloud reached 8 nm. The photoelectron cascade is bigger than a typical nanocrystal under consideration here.

The average time for the first collisional ionization scales with the primary electron energy (Figure 2). The electron cloud initiated by a photoelectron thermalizes slower than electrons in Auger cascades, since energetic electrons travel further between scattering events in the crystal due to their lower interaction cross section (Figure 3). At the same time, the cloud generated by a photoelectron is around 4 orders of magnitude larger in volume than the Auger electron induced cloud. After thermalization, the electron clouds keep expanding through diffusion, following a random walk pattern. Figure 3 shows that the radius of gyration (eq 1) at these impact energies describes well the spatial extent of the electron clouds. In Figure 3, the 4π integration over the radius at a fixed time in the 3D volume gives the total number of electrons, assuming spherical symmetry when the cascades are added stochastically.

In a sample that is small compared to the size of the X-ray beam or the photon absorption length, photoionization events will occur with equal probability throughout the entire sample. At 8.3 keV photon energy, a single photoelectron will liberate about 400 electrons before reaching thermal equilibrium (Figure 2). The electron gas will have high temperature due to the high photon energy, and the electrons will be distributed approximately uniform throughout the sample. The free electrons will scatter predominantly

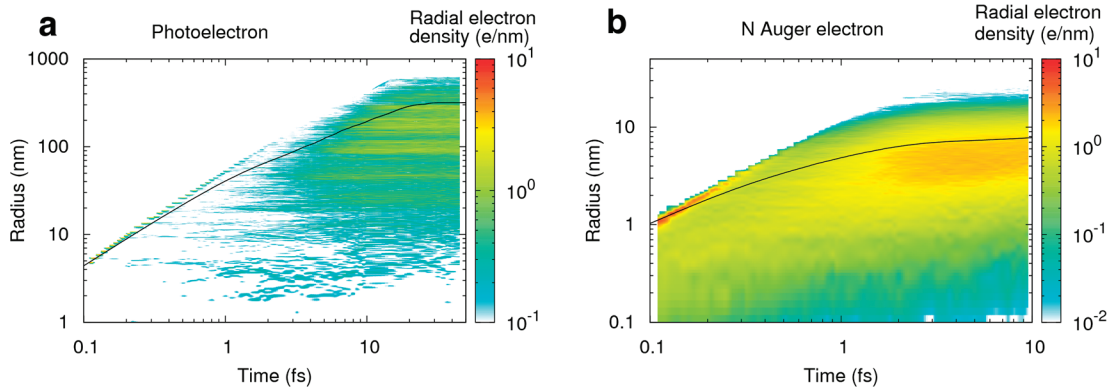

Figure 3. Spacial evolution of the electron clouds. (a) Cloud from a single photoelectron of 8 keV energy in an infinitely large urea crystal depicted through the radial electron density as a function of time and radial distance from the point of incidence. (b) Secondary electron cloud from a single Auger electron (nitrogen). The thermalization of electrons from oxygen and carbon has similar features. Black lines show the radii of gyration (eq 1) of the electron clouds. In the first femtosecond the electron clouds are highly anisotropic. After 20 fs no more secondary ionizations will occur in the photoelectron cascade (5 fs for Auger cascades). All cascades include the primary electron and its secondary electrons. Figures show averaging over 1000 simulations on an infinitely large urea crystal.

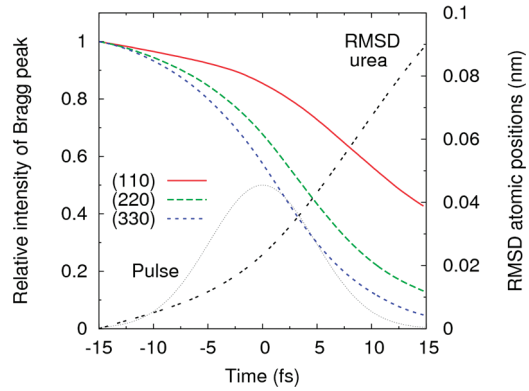

Figure 4. Decay of Bragg peaks during exposure to an X-ray pulse in a urea crystal. Pulse length: 10 fs (FWHM) centered at $t = 0$, at 1.5 Å wavelength. The pulse intensity (1.5×10^{11} photons in a focal spot of 1 μm diameter FWHM) is such that atoms are ionized once in average when 99.5% of the intensity of the pulse passes through the sample. Peak intensities at different resolutions are represented by the (hkl) reflections and are normalized to 1, based on intensities from undamaged crystals. The (330) reflection corresponds to 1.2 Å resolution and has a pulse-integrated degradation of 50% due to ionization and atomic displacement. The dashed black line shows the average root-mean-square deviations (RMSD) in atomic positions during illumination.

in the forward direction and contribute incoherently to the background in the diffraction pattern.

At 1.5 Å wavelength, the ratio between elastically scattered photons and photoionization is 1:32 for oxygen, 1:26 for nitrogen, and 1:20 for carbon. Incoming photons will primarily ionize sample and only a few will contribute to coherent scattering. The loss of an electron will decrease the scattering power by 17% for a carbon atom, 14% for nitrogen, and 12% for oxygen. One ionization per atom also leads to atomic displacement and further degradation of the scattered signal (Figure 4).

Since a focused X-ray pulse will destroy the sample, three-dimensional (3D) structure determination relies on the experiment being repeatable. Rather than building up a complete X-ray diffraction data set by rotating the crystal and collecting a sequence of diffraction images, it will be necessary to scale together individual diffraction images from many different nanocrystals, in order to assemble a complete 3D data set.[26] A crystal with $5 \times 5 \times 5$ unit cells will produce a discrete diffraction pattern,[8] and conventional X-ray analysis techniques may be used for indexing, merging, and reconstruction.[26] Furthermore, oversampling techniques for direct phase retrieval may also be employed for a 3D structural determination.[27]

To put damage caused by secondary ionization into a perspective of what resolution one can expect to achieve in the reconstructed structure, damage needs to be related to elastic photon scattering. We express damage-induced errors in terms of degradation of Bragg peaks (Figure 4), and for the entire diffraction pattern we calculate an R-value from simulated crystals exposed to X-ray pulses (Figure 5). The R-value is a measure of the overall agreement between the crystallographic model and the experimental X-ray diffraction data (eq 3). Small molecules (such as urea) form more ordered crystals and an R-value below 0.05 is considered a good threshold (Cambridge Structural Database). For macromolecules, values up to 0.20 are acceptable (Protein Data Bank), and we use the convention $R <$ 0.15 as was done by Neutze *et al.*[8] (Figure 5). Figure 4 shows how Bragg peaks may degrade during exposure to an X-ray pulse, and how this influences the dependence of the R-value with pulse parameters. The R-value is also dependent on crystal size, and Figure 5 compares two regimes: crystals where Auger cascades dominate *versus* crystals where damage is driven by photoelectron cascades. Trapping of photoelectrons in crystals larger than 500 nm leads to a steeper degradation of the signal and constrains what pulse lengths and intensities could be used for successful imaging.

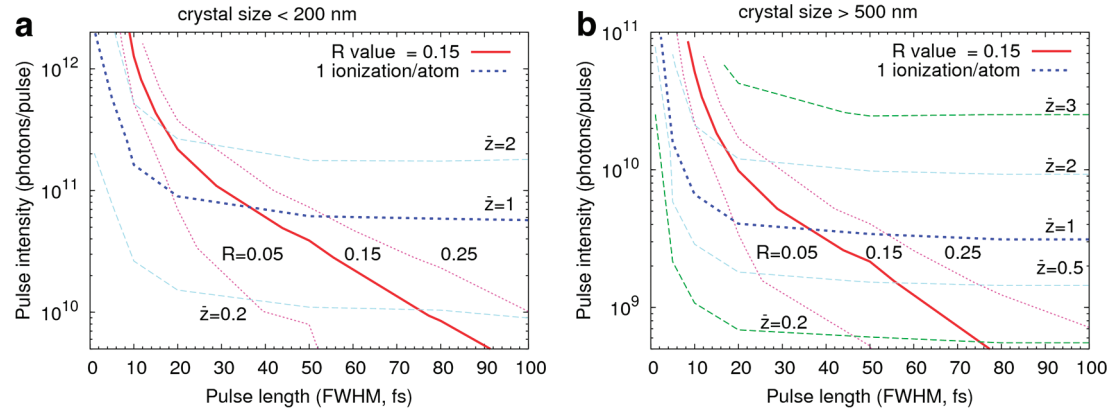

Figure 5. Degradation of the signal as a result of radiation damage. Contour plots for the average ionization per atom ($\bar{z}$) and the R-value are shown as a function of the X-ray pulse length and intensity (photons/focal spot of 1 μm diameter FWHM). The R-value (eq 3) is calculated from all the Bragg peaks up to a resolution of 1.5 Å. The red thick line corresponds to an R-value of 0.15, lower values are considered acceptable for a good reconstructable signal. The blue thick dashed line represents the damage of 1 ionization per atom. The plot in panel a shows behavior of nanocrystals smaller than 200 nm, from which the photoelectrons escape early in an exposure, while panel b shows the behavior of crystals larger than 500 nm, when photoelectrons are completely trapped during exposure.

Figure 4 presents the impact on the signal of one ionization per atom on average. At this ionization level, the scattering power of the atoms is reduced, leading to a drop of up to 30% of scattered intensity. Such a drop can be corrected and accounted for by employing correction algorithms on diffraction patterns based on statistical methods.[28] At the same time, ionization leads to destruction of the crystalline order and loss of signal in the Bragg peaks. An increase in photon flux mandates a reduction of pulse length in order to limit radiation damage (Figure 5).

We model the photon noise to be statistical noise with the signal following Poisson distribution and exemplify different requirements for the minimum number of photons per Bragg peak: 1, 10, and 100 photons. We use a criterion for signal detection when full Bragg peaks are recorded in single exposure, as a result of the intrinsic bandwidth and divergence of the X-ray source (see Methods). At 10 photons per peak it should be possible to detect a diffraction peak, even without averaging over many diffraction images. Using indexing algorithms and averaging over many exposures, one could detect Bragg peaks even with a photon signal below 1 in a single image.[26,29]

X-ray free electrons lasers are expected to deliver monochromatic X-ray pulses, with a very low spectral bandwidth $\Delta\lambda/\lambda < 0.1\%$, and with a small angular divergence ($<$1 mrad). These small spectral and angular spreads will lead to a narrow integration volume in the Fourier space which will contribute to the scattering amplitude. Thus, the diffraction patterns from single exposures will contain many partially integrated Bragg peaks. The criterion for a good exposure is chosen for fully reflected Bragg peaks in a single shot. Equation 5 is used to account for the general X-ray beam properties and gives the number of scattered photons from the incident X-ray beam for the full Bragg reflections in a single exposure. This provides a tool to map the parameter space (crystal dimensions, unit cell size, pulse parameters), to obtain structure at high resolution. Assuming an R-value of 0.15, one can predict the maximum crystal size where ionization damage is kept below a certain ionization threshold, corresponding to the desired R-value.

The signal scales with the X-ray fluence (eq 5), thus the "1" line in Figure 6 will also correspond to 10 scattered photons for the case of 10^{12} incident photons, and the "100" line will correspond to 10 scattered photons for the case of 10^{10} incident photons. If larger bandwidth or divergence is expected, full Bragg peaks can be recorded at lower resolutions and consequently the detected signal will be higher (eq 5).

Identical number of unit cells give bigger crystals with macromolecules than with small molecules, while maintaining a similar electron density. This affects size-dependent damage processes. Since high-energy electrons thermalize rather slowly, the shorter the pulse, the larger the molecule that can be imaged. Our simulations are done for pulses up to 100 fs long. A single protein molecule, hit with a 100 fs, 10^{10} photons/μm^2 pulse will be completely destroyed after the pulse.[8] Theoretical calculations have shown that due to the shielding of the ionized atoms by free electrons in the sample, the explosion starts from the surface of the sample and travels inward to the core.[15,16] Thus, the inner part of the sample does not show expansion during the initiating state of the explosion. For example, a carbon cluster of 60 Å radius illuminated by a 1.5×10^{11} photons/fs/(100 nm)^2 pulse for 60 fs shows hardly any radial expansion inside a 45 Å radius core, which remains neutral.[16] This implies that for a crystal of the same size, or larger, exposed to a similar pulse, there is no expansion of the unit cells in the inner part of crystal. Hence, crystalline diffraction and useful structural information might still be obtained from the center of the crystal.

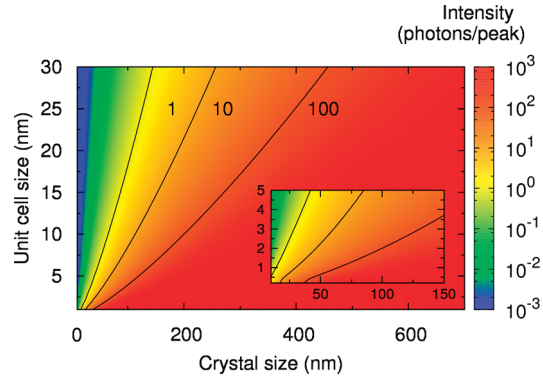

Figure 6. Photon signal as a function of unit cell and crystal size for a perfect crystal. The integrated Bragg peak intensity (eq 5) is shown for the lowest resolution where a full reflection can be recorded (eq 4). Fully integrated Bragg peaks from single exposures can be used for indexing and averaging the signal from different nanocrystal orientations in the beam, and 10 detected photons are considered to give a good signal-to-noise ratio. The X-ray pulse has an intensity of 10^{11} photons focused in a focal spot of 1 μm diameter (FWHM), a wavelength of 1.5 Å, a beam divergence of 1 mrad, and a spectral bandwidth, $\Delta\lambda/\lambda$, of 0.1%. The solid lines correspond to a scattered signal of 1, 10, and 100 photons in the first fully integrated Bragg peak, when peak degradation is not taken into account. The inset shows details for crystals with small unit cells.

Considering a photon pulse containing 10^{11} photons, that is focused to a spot of 1 μm diameter, a perfect crystal of deacetoxycephalosporin, DAOCS (1UNB)[30] (an average sized protein with unit cell dimensions of $a = 10.7$, $b = 10.7$, $c = 7.01$ nm), would have to be of a size below 200 nm to give a signal of 10 photons in the fully reflected Bragg peaks (Figure 6). From such a small crystal most electrons generated from the photoelectron would escape. To get an *R*-value below 0.15, the pulse length would have to be less than 30 fs (FWHM) (Figure 5a).

For a molecule of the unit cell size of urea (Figure 6, inset), a 50 nm perfect crystal would give an image with

an *R*-value of 0.15, using a 10^{10} photon pulse, with a focal spot of 1 μm diameter and a pulse length of 75 fs. For a 30 nm crystal the number of photons would have to be increased above 10^{11} and the pulse length would have to be shorter than 30 fs.

CONCLUSIONS

We present a theoretical study of the dynamics of the electrons generated in a biological sample placed in an XFEL beam, based on simulations of electron impact ionization and cascade development in urea crystals. Owing to the higher inelastic electron cross section at lower energies,[21] the secondary cascade caused by an Auger electron is generated faster than the corresponding cascade from the photoelectron (Figure 2). The electron density associated with the Auger cloud is higher and more localized around the point where the initial electron was created (Figure 1). This leads inherently to two secondary electron energy regimes and two electron cloud sizes, which occur simultaneously in the sample during the exposure.

When deciding which parameters of the X-ray laser pulse and sample characteristics one should use (Figure 6), there is an interplay between two effects driven mainly by photoelectrons; (i) If photoelectrons escape the sample, the total number of ionizations will be significantly lowered. To reduce radiation damage early in the exposure, the sample has to be smaller than the size of the photoelectron cascade. The diffraction signal from the crystal scales with the size of the crystal as a power law (eq 5); thus, reducing sample size will conversely require an increase in pulse intensity in order to retain the signal at the same level (Figure 6). (ii) If the pulse is very short, the photoelectric cascade will not have time to develop to reach a large number of ionizations. At the same time, short pulses considerably reduce the signal degradation due to atomic displacements and ionization (low *R*-value in Figure 5). In this case the sample size is less important, and one can investigate any crystal size at photon fluences that will provide enough signal. The size could however be constrained by coherence requirements due to the pulse length.[23] At extremely short pulses, one would also need to consider the broadening of Bragg peaks,[31] that is, a bandwidth effect.

The above considerations stress the importance of having very short pulses as means for radiation damage control, to reduce both the ionization cascades and the atomic disorder. A photon flux of 10^{12} photons per pulse and unit area (μm^2) will offer the opportunity to investigate a wider range of crystal sizes and unit cells sizes. For lower available intensities (10^{10} photons/pulse), longer pulse lengths can be accommodated and imaging nanocrystals of small proteins with a small unit cell, such as lysozyme, could be feasible. Our calculations show that to achieve an *R*-value of 0.15 at a fluence of 10^{11} photons/μm^2 pulses have to be shorter than 10 fs for crystals larger than 500 nm, whereas for small crystals (<200 nm) pulse lengths can be as long as 30 fs.

Ultrafast single-shot nanocrystallography fills the gap between single molecule imaging and crystallography. It offers the opportunity to investigate biological molecules which are too small to provide a good signal on their own in an X-ray laser diffraction experiment, however they could form nanocrystals which would be too small to investigate with conventional synchrotron radiation. Our calculations show that pulses of 10^{11} photons/μm^2 provide an ideal case for nanocrystal imaging. This number is well within the range of various X-ray lasers and early operational parameters. The near future holds the prospect of structural determination from submicrometer protein crystals.

METHODS

Electron Impact Ionization. Simulations of the ionization cascade dynamics in crystalline urea ($CO(NH_2)_2$) were performed using the spatial electron dynamics program, EHOLE, that is a part of the GROMACS[32] Molecular Dynamics (MD) software package. Urea was chosen as a model for a biological sample for three reasons: it has a well-known crystalline structure, it has an atomic composition of biological character, and its unit cell is small. In earlier work,[21] the inelastic electron cross sections for urea were derived from first principles calculations. On the basis of these we have calculated the number of secondary electrons generated by an impact electron in a urea crystal. The inelastic cross section for electron scattering in urea is comparable in magnitude with that for water.[21] Thus, urea crystals are a good model for protein nanocrystals, known to contain 30%−60% water. We refer to refs 21, 25, and 33 and the Supporting Information for further details of these calculations and how the model compares with experiments on diamond.[34] Considering $\mathbf{r}_i$ to be the position of electron *i* with respect to the center of mass of all free electrons and $N(t)$ the total number of electrons at a certain time, the radius of gyration, used in Figure 3, is defined as

$$R_g(t) = \left(\frac{1}{N(t)}\sum_i \mathbf{r}_i(t)^2\right)^{1/2} \quad (1)$$

Electron Thermalization during the Pulse. We assume that the X-ray pulse can be described by a Gaussian centered at time $t_0 = 0$ and will consider the incoming X-ray photons to be unpolarized and have a wavelength of 1.5 Å. Following this pulse, several primary ionizations are treated—the photoelectric effect resulting in an ejection of a high energy electron (~8 keV), accompanied by an Auger effect which provides an electron of a lower energy, depending on atomic species. The emission for these electrons is described by normalized probability distributions: (i) the photoelectric effect is instantaneous so the emission probability follows the same Gaussian profile as the X-ray pulse, with the width *w*; (ii) the probability for an Auger process to be emitted is a convolution of a Gaussian with the exponential decay characteristic for each individual atomic species. The exponential decays are taken with corresponding life times τ of 11.3 fs for carbon, 8.3 fs for nitrogen, and 6.6 fs for oxygen. The probability for photoionization in urea is determined by the cross section of the atoms, which are well-known. For the three atomic species that can undergo an Auger process, the contribution from the atoms C, N,

and O, is weighted according to the photoionization cross section on the respective atoms, σ_C, σ_N, σ_O, and normalized to the total photoelectric cross section for the urea molecule. The single electron ionization cascades develop mainly along the direction of the incident electron, however we consider spherical symmetry when these are stochastically produced. Thus, the entire ionization cascade following an X-ray pulse impinging on a crystal is given by

$$C(t) = \sum_{i=C,N,O} n_i\sigma_i\left\{\int Ne^{-(t'-t_0)^2/(2w^2)}C_{photo}(t,t')\,dt' + \int Ne^{-(t'-t_0)^2/(2w^2)}\frac{1}{\tau}e^{-(t-t')/\tau}C_{Auger}(t,t')\,dt'\right\} \quad (2)$$

where $C_{photo}(t,t')$ and $C_{Auger}(t,t')$ generally represent the cascade development with time for a single electron starting from time t'. These functions are obtained from MD simulations separately for photoelectrons and Auger electrons. For example, these functions could represent the ionization rate as a function of time from photoelectrons or Auger electrons $N(t,t')$ following the creation of the initial electron at time t' (Figure 2 shows $N(t,t' = 0)$). Another example is the radius of gyration $R_g(t,t')$ from individual photoelectrons and Auger electrons created at time t', shown in Figure 3 for $R_g(t,t' = 0)$.

X-ray Interactions and Damage Quantification. The degradation of Bragg peaks in Figure 4 and Figure 5 has been calculated from MD simulations on an urea crystal, using GROMACS with a stochastic interaction of X-ray photons with atoms, assuming unpolarized X-rays and homogeneous spatial distribution of the free electrons. The simulation box was $10 \times 10 \times 10$ unit cells of urea, with periodic boundary conditions, and includes thermal motion of atoms. The model is described in ref 8 and in the Supporting Information. The intensity of Bragg peaks at each time step is defined by integrating around each peak over a rectangular area centered on the Bragg peak and with sides of length equal to 1/10 of the separation between adjacent peaks.[11] The spectral width $\Delta\lambda/\lambda$, beam divergence or any broadening of the Ewald sphere are not taken into account here. The degradation of the Bragg peak is expected to be smaller when integrating through an Ewald sphere of finite thickness. To estimate the damage induced error we make use of the *R*-value (used in Figure 5), calculated up to a resolution $\boldsymbol{q}$ from

$$R(q) = \frac{\sum_{hkl<q}|\sqrt{\langle I_{hkl}\rangle_t} - \sqrt{I^0_{hkl}}|}{\sum_{hkl<q}\sqrt{\langle I_{hkl}\rangle_t}} \quad (3)$$

where the summation is performed over all Bragg peaks (hkl) corresponding to scattering vectors less than $\boldsymbol{q}$. The intensities of the Bragg peaks I^0_{hkl} for the undamaged crystal are used as reference when compared with the time averaged intensities $\langle I_{hkl}\rangle_t$ of the damaged crystal exposed to a Gaussian-shaped X-ray pulse. The latter intensities take into account the ionization dynamics and atomic displacement as a function of time during the X-ray pulse.

Minimum Required Signal. In ultrafast single-shot experiments at X-ray lasers the crystals will be exposed in random orientations, X-rays beams are expected to have small divergence (<1 mrad) and are nearly monochromatic (spectral bandwidth $\Delta\lambda/\lambda < 0.1\%$). Thus, single shot diffraction patterns will contain many partially reflected Bragg peaks. Full Bragg peaks may be recorded on the detector at higher resolution and could be used for retrieving the original orientation of the nanocrystals and for averaging the signal from similar orientation[26] (partial Bragg peaks could in principle also be used for indexing). In our estimates for the minimum required signal for successful indexing, we consider only the signal from fully integrated Bragg peaks at the lowest resolution where these can be recorded. For given parameters that control the thickness of the Ewald sphere (beam divergence $\Delta\phi$, spectral bandwidth $\Delta\lambda/\lambda$), the lowest resolution where a full Bragg peak can be recorded (q_{min}) is found by comparing the thickness of the Ewald sphere to the size of the Bragg peak (modeled as inversely proportional to the crystal width *A*)

$$\frac{1}{A} \sim \left|\frac{\Delta\lambda}{\lambda}\frac{\lambda}{2}q^2_{min} - \Delta\phi q_{min}\sqrt{1 - \frac{\lambda^2}{4}q^2_{min}}\right| \quad (4)$$

For most of the X-ray lasers, the main contribution is expected to come from the divergence. This equation can be applied to less monochromatic light sources, where the spectral bandwidth could give a dominant contribution. Further details can be found in the Supporting Information.

The average number of photons scattered elastically by a protein crystal within a Bragg peak for a given resolution q_{min} can be approximated by the expression for the integrated reflected intensity[35]

$$I_{Bragg}(q_{min}) \approx I_0\frac{\lambda^3}{\sin\theta_0}\frac{1+\cos^2\theta_0}{2} \times \lambda^2\frac{A^3}{a^6}r_e^2\sum_{atoms}f^2_{atom}(\theta_0) \quad (5)$$

where both small beam divergence and near monochromaticity are accounted for. I_0 is the intensity of the incoming X-ray beam (number of incoming photons per unit area), integrated over the angular density of the incident beam. The Lorentz factor $\lambda^3/\sin\theta_0$ takes into account the integration over the thickness of the Ewald sphere encompassing the Bragg peak, in a similar way as[35] for the stationary case (no rotation) with divergent monochromatic radiation. The polarization factor is given by $(1 + \cos^2\theta_0)/2$. Furthermore, r_e is the classical electron radius, λ is the wavelength, *A* is the crystal side (cubic crystal), *a* is the unit cell side (cubic unit cell), f_{atom} is the atomic scattering factor, and θ_0 is the polar angle between the incident pulse and the center of the Bragg peak.

It is assumed that the unit cell structure factor is constant within the Bragg peak, and that adjacent Bragg peaks do not overlap; both these approximations improve with the ratio *A*/*a*. The squared structure factor of the unit cell is represented by its average value at high scattering angles.[36] For numerical evaluation, the unit cell was assumed to have a density of 1/30 Å^{-3} carbon-equivalent atoms (corresponding to a unit cell consisting of 50% nonstructural water and protein with a density approximately equal to 1.35 g/cm^3), and the scattering factor of carbon was calculated from the Cromer−Mann parameters.[37] The calculation of the number of photons per Bragg peak (eq 5) is presented in Figure 6 with the assumption of perfect crystals with no mosaicity. It has been shown that micrometer sized crystals could consist of only a few highly ordered domains,[38] thus nanocrystals are unlikely to be organized with a mosaic spread.

The above approximations will break down when the crystal size approaches the unit cell size, as the diffracted image turns from a discrete into a continuous pattern.

Acknowledgment. The Swedish Research Council is acknowledged for financial support as well as the DFG Cluster of Excellence: Munich-Center for Advanced Photonics. The authors would like to thank Magnus Bergh, Gerard Kleywegt, Inger Andersson, Erik G. Marklund, Richard Neutze, Martin Svenda, Rosmarie Friemann, Jochen Hub, and Karin Valegård for their valuable input.

Supporting Information Available: Extended description of the methods: detailed description of the free electron cloud calculations, the estimation of radiation damage induced by ionization and atomic displacements, and a formal derivation of the conditions for integrated reflections. This material is available free of charge *via* the Internet at http://pubs.acs.org.

REFERENCES AND NOTES

1. Ackermann, W.; Asova, G.; Ayvazyan, V.; Azima, A.; Baboi, N.; Bahr, J.; Balandin, V.; Beutner, B.; Brandt, A.; Bolzmann, A.; *et al*. Operation of a Free-Electron Laser from the Extreme Ultraviolet to the Water Window. *Nat. Photonics* **2007**, *1*, 336–342.
2. DiMauro, L. F.; Arthur, J.; Berrah, N.; Bozek, J.; Galayda, J. N.; Hastings, J. Progress Report on the LCLS XFEL at SLAC. *J. Phys., Conf. Ser.* **2007**, *88*, 012058.

3. Shintake, T.; Tanaka, H.; Hara, T.; Tanaka, T.; Togawa, K.; Yabashi, M.; Otake, Y.; Asano, Y.; Bizen, T.; Fukui, T.; *et al*. A Compact Free-Electron Laser for Generating Coherent Radiation in the Extreme Ultraviolet Region. *Nat. Photonics* **2008**, *2*, 555–559.
4. Altarelli, M.; Brinkmann, R.; Chergui, M.; Decking, W.; Dobson, B.; Düsterer, S.; Grübel, G.; Graeff, W.; Graafsma, H.; Hajdu, J.; *et al*. *The European X-Ray Free-Electron Laser Technical Design Report;* DESY XFEL Project Group: Hamburg, Germany, 2007; DESY 2006-097.
5. Leemans, W. P.; Geddes, C. R.; Faure, J.; Tóth, C.; van Tilborg, J.; Schroeder, C. B. ; Esarey, E.; Fubiani, G.; Auerbach, D.; Marcelis, B.; *et al*. Observation of Terahertz Emission from a Laser-Plasma Accelerated Electron Bunch Crossing a Plasma-Vacuum Boundary. *Phys. Rev. Lett.* **2003**, *91*, 074802.
6. Günter, F.; Becker, S.; Schramm, U.; Eichner, T.; Fuchs, M.; Weingartner, R.; Habs, D.; Meyer-ter-vehn, J.; Geissler, M.; Ferrario, M.; *et al*. Design Considerations for Table-Top, Laser-Based VUV and X-ray Free Electron Lasers. *Appl. Phys. B: Laser Opt.* **2007**, *86*, 431–435.
7. Ravasio, A.; Gauthier, D.; Maia, F. R. N. C.; Billon, M.; Caumes, J. P.; Garzella, D.; Geleoc, M.; Gobert, O.; Hergott, J. F.; Pena, A. M.; *et al*. Single-Shot Diffractive Imaging with a Table-Top Femtosecond Soft X-ray Laser-Harmonics Source. *Phys. Rev. Lett.* **2009**, *103*, 028194.
8. Neutze, R.; Wouts, R.; van der Spoel, D.; Weckert, E.; Hajdu, J. Potential for Biomolecular Imaging with Femtosecond X-ray Pulses. *Nature* **2000**, *406*, 752–757.
9. Neutze, R.; Huldt, G.; Hajdu, J.; van der Spoel, D. Potential Impact of an X-ray Free Electron Laser on Structural Biology. *Radiat. Phys. Chem.* **2004**, *71*, 905–916.
10. Boutet, S.; Robinson, I. Coherent X-ray Diffractive Imaging of Protein Crystals. *J. Synchrotron Radiat.* **2008**, *15*, 576–583.
11. van der Spoel, D.; Maia, F. R. N. C.; Caleman, C. Structural Studies of Melting on the Picosecond Time Scale. *Phys. Chem. Chem. Phys.* **2008**, *10*, 6344–6349.
12. Hau-Riege, S. P.; London, R. A.; Bionta, R. M.; McKernan, M. A.; Baker, S. L.; Krzywinski, J.; Sobierajski, R.; Nietubyc, R.; Pelka, J. B.; Jurek, M.; *et al*. Damage Threshold of Inorganic Solids under Free-Electron-Laser Irradiation at 32.5 nm Wavelength. *Appl. Phys. Lett.* **2007**, *90*, 173128.
13. Chalupský, J.; Juha, L.; Kuba, J.; Cihelka, J.; Hajkova, V.; Koptyaev, S.; Krasa, J.; Velyhan, A.; Bergh, M.; Caleman, C.; *et al*. Characteristics of Focused Soft X-ray Free-Electron Laser Beam Determined by Ablation of Organic Molecular Solids. *Opt. Express* **2007**, *15*, 6036–6043.
14. Hau-Riege, S. P.; London, R. A.; Bionta, R. M.; Ryutov, D.; Soufli, R.; Bajt, S.; McKernan, M. A.; Baker, S. L.; Krzywinski, J.; Sobierajski, R.; *et al*. Wavelength Dependence of the Damage Threshold of Inorganic Materials under Extreme-Ultraviolet Free-Electron-Laser Irradiation. *Appl. Phys. Lett.* **2009**, *95*, 111104.
15. Bergh, M.; Timneanu, N.; van der Spoel, D. A Model for the Dynamics of a Water Cluster in a X-ray FEL Beam. *Phys. Rev. E* **2004**, *70*, 051904.
16. Hau-Riege, S. P.; London, R. A.; Szöke, A. Dynamics of Biological Molecules Irradiated by Short X-ray Pulses. *Phys. Rev. E* **2004**, *69*, 051906.
17. Jurek, Z.; Faigel, G.; Tegze, M. Dynamics in a Cluster Under the Influence of Intense Femtosecond Hard X-ray Pulses. *Eur. Phys. J. D* **2004**, *29*, 217–229.
18. Nave, C.; Hill, M. A. Will Reduced Radiation Damage Occur with Very Small Crystals. *J. Synchrotron Radiat.* **2005**, *12*, 299–303.
19. Cowan, J. A.; Nave, C. The Optimum Conditions to Collect X-ray Data from Very Small Samples. *J. Synchrotron Radiat.* **2008**, *15*, 458–462.
20. *X-ray Data Booklet*, 2nd ed.; Thompson, A. C., Vaughan, D., Eds.; Lawrence Berkeley National Laboratory: Berkeley, CA, 2001.
21. Caleman, C.; Ortiz, C.; Marklund, E.; Bultmark, F.; Gabrysch, M.; Parak, F. G.; Hajdu, J.; Klintenberg, M.; Timneanu, N. Radiation Damage in Biological Material, Electronic Properties and Electron Impact Ionization in Urea. *Europhys. Lett.* **2009**, *85*, 18005. Erratum: *Europhys. Lett.* **2009**, *88*, 29901.
22. Shapiro, D. A.; Chapman, H. N.; De-Ponte, D.; Doak, R. B.; Fromme, P.; Hembree, G.; Hunter, M.; Marchesini, S.; Schmidt, K.; Spence, J.; *et al*. Powder Diffraction from a Continuous Microjet of Submicrometer Protein Crystals. *J. Synchrotron. Radiat.* **2008**, *15*, 593–599.
23. Hau-Riege, S. P. Effect of the Coherence Properties of Self-Amplified-Spontaneous-Emission X-ray Free Electron Lasers on Single-Particle Diffractive Imaging. *Opt. Express* **2008**, *16*, 2840–2844.
24. Ziaja, B.; London, R. A.; Hajdu, J. Unified Model of Secondary Electron Cascades in Diamond. *J. Appl. Phys.* **2005**, *97*, 064905.
25. Ortiz, C.; Caleman, C. Secondary Electron Cascade Dynamics in KI and CsI. *J. Phys. Chem. C.* **2007**, *111*, 17442–17447.
26. Kirian, R. A.; Wang, X.; Weierstall, U.; Schmidt, K. E.; Spence, J. C. H.; Hunter, M.; Fromme, P.; White, T.; Chapman, H. N.; Holton, J. Femtosecond Protein Nanocrystallography—Data Analysis Methods. *Opt. Express* **2010**, *18*, 5713–5723.
27. Miao, J.; Hodgson, K. O.; Sayre, D. An Approach to Three-Dimensional Structures of Biomolecules by Using Single-Molecule Diffraction Images. *Proc. Natl. Acad. Sci. U.S.A.* **2001**, *98*, 6641–6645.
28. Hau-Riege, S. P.; London, R. A.; Chapman, H. N.; Szoke, A.; Timneanu, N. Encapsulation and Diffraction-Pattern-Correction Methods to Reduce the Effect of Damage in X-ray Diffraction Imaging of Single Biological Molecules. *Phys. Rev. Lett.* **2007**, *98*, 198302.
29. Fung, R.; Shneerson, V.; Saldin, D. K.; Ourmazd, A. Structure from Fleeting Illumination of Faint Spinning Objects in Flight. *Nat. Phys.* **2009**, *5*, 64–67.
30. Valegård, K.; Terwisscha van Scheltinga, A. C.; Dubus, A.; Rhangino, G.; Oster, L. M.; Hajdu, J.; Andersson, I. The Structural Basis of Cephalosporin Formation in a Mononuclear Ferrous Enzyme. *Nat. Struct. Biol.* **2004**, *11*, 95–101.
31. Tomov, I. V.; Chen, P.; Rentzepis, P. M. Pulse Broadening in Femtosecond X-ray Diffraction. *J. Appl. Phys.* **1998**, *83* (10), 5546–5548.
32. van der Spoel, D.; Lindahl, E.; Hess, B.; Groenhof, G.; Mark, A. E.; Berendsen, H. J. C. GROMACS, Fast, Flexible and Free. *J. Comput. Chem.* **2005**, *26*, 1701–1718.
33. Timneanu, N.; Caleman, C.; Hajdu, J.; van der Spoel, D. Auger Electron Cascades in Water and Ice. *Chem. Phys.* **2004**, *299*, 277–283.
34. Gabrysch, M.; Marklund, E.; Hajdu, J.; Twitchen, D. J.; Rudati, J.; Lindenberg, A. M.; Caleman, C.; Falcone, R. W.; Tschentscher, T.; Moffat, K.; *et al*. Formation of Secondary Electron Cascades in Single-Crystalline Plasma-Deposited Diamond upon Exposure to Femtosecond X-ray Pulses. *J. Appl. Phys.* **2008**, *103*, 064909.
35. Kalman, Z. H. On the Derivation of Integrated Reflected Energy Formulae. *Acta Cryst. A* **1979**, *35*, 634–641.
36. Wilson, A. J. C. The Probability Distribution of X-ray Intensities. *Acta Cryst.* **1949**, *2*, 318–321.
37. Cromer, D. T.; Mann, J. B. X-ray Scattering Factors Computed from Numerical Hartree−Fock Wave Functions. *Acta Cryst. A* **1968**, *24*, 321–326.
38. Fourme, R.; Ducruix, A.; Rieskautt, M.; Capelle, B. The Perfection of Protein Crystals Probed by Direct Recording of Bragg Reflection Profiles with a Quasi-planar X-ray Wave. *J. Synchrotron Radiat.* **1995**, *2*, 136–142.